





Original Article



Fucoidan Ameliorates Ferroptosis in Ischemia-reperfusion-induced Liver Injury through Nrf2/HO-1/GPX4 Activation

Jing-Jing Li^{1#}, Wei-Qi Dai^{1#}, Wen-Hui Mo¹, Wen-Qiang Xu¹, Yue-Yue Li¹, Chuan-Yong Guo^{2*} 
and Xuan-Fu Xu^{1*} 

¹Department of Gastroenterology, Shidong Hospital of Shanghai, Shanghai, China; ²Department of Gastroenterology, Shanghai Tenth People's Hospital, Tongji University School of Medicine, Shanghai, China

Received: 26 March 2023 | Revised: 17 April 2023 | Accepted: 10 May 2023 | Published online: Month 00, 2023

Abstract

Background and Aims: Liver ischemia-reperfusion (IR) injury is a common pathological process in liver surgery. Ferroptosis, which is closely related to lipid peroxidation, has recently been confirmed to be involved in the pathogenesis of IR injury. However, the development of drugs that regulate ferroptosis has been slow, and a complete understanding of the mechanisms underlying ferroptosis has not yet been achieved. Fucoidan (Fu) is a sulfated polysaccharide that has attracted research interest due to its advantages of easy access and wide biological activity. **Methods:** In this study, we established models of IR injury using erastin as an activator of ferroptosis, with the ferroptosis inhibitor ferrostatin-1 (Fer-1) as the control. We clarified the molecular mechanism of fucoidan in IR-induced ferroptosis by determining lipid peroxidation levels, mitochondrial morphology, and key pathways in theta were involved. **Results:** Ferroptosis was closely related to IR-induced hepatocyte injury. The use of fucoidan or Fer-1 inhibited ferroptosis by eliminating reactive oxygen species and inhibiting lipid peroxidation and iron accumulation, while those effects were reversed after treatment with erastin. Iron accumulation, mitochondrial membrane rupture, and active oxygen generation related to ferroptosis also inhibited the entry of nuclear factor erythroid 2-related factor 2 (Nrf2) into the nucleus and reduced downstream heme oxygenase-1 (HO-1) and glutathione peroxidase 4 (GPX4) pro-

tein levels. However, fucoidan pretreatment produced adaptive changes that reduced irreversible cell damage induced by IR or erastin. **Conclusions:** Fucoidan inhibited ferroptosis in liver IR injury via the Nrf2/HO-1/GPX4 axis.

Citation of this article: Li JJ, Dai WQ, Mo WH, Xu WQ, Li YY, Guo CY, et al. Fucoidan Ameliorates Ferroptosis in Ischemia-reperfusion-induced Liver Injury through Nrf2/HO-1/GPX4 Activation. J Clin Transl Hepatol 2023. doi: 10.14218/JCTH.2023.00133.

Introduction

Orthotopic liver transplantation, shock, abdominal surgery, and vascular embolism can cause liver ischemia-reperfusion (IR) injury.¹ In addition, as the standard treatment method for end-stage liver diseases, liver transplantation may result in liver tissue ischemia. However, after blood perfusion is restored, organ function may deteriorate further, which seriously restricts the therapeutic effect of liver transplantation.^{2,3} Therefore, it is extremely important to find ways to pre-adapt the body and reduce injury based on the pathogenesis of IR.⁴

The mechanism of liver IR injury is complex, involving almost all types of hepatocytes and infiltrating neutrophils, macrophages, and platelets.⁵ Iron-dependent biological activities may also be involved in the pathogenesis of IR injury.^{6,7} In 2012, Dixon *et al.*⁸ studied the mechanism of erastin inducing cell death through the RAS gene mutation and discovered ferroptosis, a new type of programmed cell death mediated by iron ions.⁹ Research has shown that ferroptosis is an important link in the pathophysiology of IR injury in various organs.¹⁰ In the liver, Wu *et al.*¹¹ demonstrated that the level of ferroptosis increased in patients with hepatectomy and in mice with liver IR, and ferrostatin-1 (Fer-1) reduced liver injury induced by IR. The results showed that regulating ferroptosis to interfere with IR may provide new research ideas and treatment strategies for the treatment of liver IR injury.

Fucoidan, a sulfated polysaccharide from the sea, is mainly present in the cell wall matrix of various brown algae, is widely sourced, and has a variety of biological and pharmacological activities.¹²⁻¹⁷ Fucoidan does not have significant toxicity in rats, and volunteers who ingested 3 g of 75% fucoidan capsules for 12 days experienced no side effects or toxicity.¹⁸⁻²¹ Studies have confirmed that fucoidan supple-

Keywords: Fucoidan; Ischemia-reperfusion; Ferroptosis; Lipid peroxidation; Nrf2.

Abbreviations: ALT, Alanine transaminase; AST, Aspartate Transaminase; ATF4, Activating Transcription Factor 4; DEGs, Differentially expressed genes; DHE, Dihydroethidium; Er, Erastin; FANCD2, Fanconi anemia, complementation group D2; Fer-1, ferrostatin-1; FTH1, ferritin heavy polypeptide 1; Fu, Fucoidan; GAPDH, glyceraldehyde-3-phosphate dehydrogenase; GCH1, GTP cyclohydrolase 1; GPX4, glutathione peroxidase; GSH, L-Glutathione; HE, Hematoxylin-eosin staining; HO-1, Heme oxygenase-1; IR, Ischemia-reperfusion; LDH, Lactic dehydrogenase; MDA, Malonaldehyde; Nrf2, Nuclear factor erythroid 2-related factor 2; PCR, Polymerase chain reaction; PRKAA2, protein kinase AMP-activated catalytic subunit alpha 2; ROS, Reactive oxygen species; SQSTM1, Sequestosome 1; SREBF1, Sterol Regulatory Element Binding Transcription Factor 1; TEM, Transmission electron microscope; TFAP2A, Transcription Factor AP-2 alpha; TFRC, Transferrin receptor.

*Contributed equally to this work.

***Correspondence to:** Chuan-Yong Guo, Shanghai Tenth People's Hospital, 301 Yanchang Road, Jingan District, Shanghai, China. ORCID: <https://orcid.org/0000-0002-6527-4673>. Tel: +86-21-66300588, E-mail: guochuanyong@hotmail.com; Xuan-Fu Xu, Shidong Hospital of Shanghai, 999 Shiguang Road, Yangpu District, Shanghai, China. ORCID: <https://orcid.org/0000-0002-5538-6591>. Tel: +86-21-25066666, E-mail: shuanfusky@163.com

mentation protects liver cells from ferroptotic damage caused by long-term alcohol exposure by inhibiting iron overload and liver oxidative damage.²² In a previous study, we found that fucoidan also had antioxidant activity, so we have reason to believe that it protects against IR-induced injury.^{14,23} In this study, we used a variety of molecular biological experiments to verify that the injury induced by ferroptosis was reduced by fucoidan activation of the Nrf2/HO-1/GPX4 axis.

Methods

Animals and cell culture

Six- to eight-week-old male Balb/C mice weighing 20–25 g were purchased from Shanghai SLAC Laboratory Animal Co. Ltd. (Shanghai, China). The mice were housed in clean cages with a 12 h alternating light/dark cycle at a constant temperature of 22–25°C and were given free access to food and water until the start of fasting 12 h before surgery. Normal human hepatocyte LO2 cells were purchased from the Cell Bank of Type Culture Collection (Chinese Academy of Sciences, Beijing, China) and cultured in RPMI 1640 medium (Sigma-Aldrich Corp., St. Louis, MO, USA) with 10% fetal bovine serum, 100 IU/mL penicillin and 100 mg/mL streptomycin in 5% CO₂ and at 37°C in a humidified incubator. The experiment protocol was conducted according to the Declaration of Helsinki with the approval of the Shidong Hospital Research Ethics Committee (No. 2020-0002).

Mouse model of IR injury and experimental design

A 70% liver IR model was established as previously described.^{24,25} A total of 108 mice were randomly divided into six groups of 18 each:^{14,23} (1) Sham, an equivalent volume of normal saline as received by the IR group was delivered for 2 weeks by gavage before on-off of abdomen; (2) Fucoidan (Fu), fucoidan (40 mg/kg for 2 weeks) by gavage before on-off of abdomen; (3) IR, an equal volume of normal saline for 2 weeks by gavage before IR operation; (4) IR+Fu, fucoidan (40 mg/kg for 2 weeks) by gavage before IR operation; (5) IR+Fu+Erastin (Er), fucoidan (40 mg/kg for 2 weeks) by gavage and erastin (100 mg/kg, four times at 12 h intervals) by intraperitoneal injection before IR operation; and (6) IR+Fer-1, an equal volume of normal saline for 2 weeks) by gavage and Fer-1 (1 mg/kg, once at 48 h) by tail vein injection before IR operation (Fig. 1B). Six mice in each group were euthanized at 4, 8, and 24 h after IR and serum and liver tissue were collected for further experiments.

Cell model of hypoxia-reoxygenation (HR) injury and experimental design

We simulated IR injury *in vitro* by treating normal hepatocytes with hypoxia and reoxygenation.²⁶ We placed proliferating LO2 cells in a three-gas tank (oxygen concentration <1%) in glucose-free RPMI-1640 medium for 3 h, and then transferred them back to the normal incubator for 6 h before conducting subsequent experiments. The cell groups were: (1) Normal culture (NC) conditions; (2) Fu, fucoidan treatment (50 µg/mL for 2 h); (3) C-IR, HR treatment; (4) C-IR+Fu, fucoidan pretreatment (50 µg/mL for 2 h) before HR treatment; (5) C-IR+Fu+Er, fucoidan (50 µg/mL for 2 h) and erastin (10 µM for 1 h) pretreatment before HR treatment; (6) C-IR+Fer-1, Fer1 pretreatment (2 µM for 12 h) before HR treatment.

Chemicals and reagents

Fucoidan (Cat. No. F8190) was purchased from Sigma-Al-

drich dissolved in normal saline or phosphate-buffered saline (PBS) and was prepared as a mother liquor at a concentration of 20 mg/mL and stored at 4°C refrigerator. Fer-1 (Cat. No. HY-100579), erastin (Cat. No. HY-15763) and MG-132 (Cat. No. HY-13259) were obtained from MedChemExpress (Monmouth Junction, NJ, USA). Alanine transaminase (ALT; Cat. No. C009-2-1), aspartate aminotransferase (AST; Cat. No. C010-2-1), Lactate dehydrogenase (LDH; Cat. No. A020-2-2), (GSH; glutathione, Cat. No. A006-2-1), malondialdehyde (MDA; Cat. No. A003-4-1) and tissue iron (Cat. No. A039-2-1) microplate assay kits were from Jancheng Biotech (Nanjing, China). Staining solutions for hematoxylin and eosin (HE, Cat. No. C0105), oil red O (Cat. No. C0157), reactive oxygen species (ROS; Cat. No. S0033), Mito-Tracker Green (Cat. No. C1048), and nuclear and cytoplasmic protein extraction kits (Cat. No. P0027) were purchased from Beyotime (Shanghai, China). FerroOrange (Cat. No. F374) and cell counting kit (CCK)-8 were obtained from Dojindo Laboratories (Tokyo, Japan). Antibodies, including ubiquitin (Cat. No. 10201-2-AP), Nrf2 (Cat. No. 16396-1-AP), HO-1 (Cat. No. 10701-1-AP), GPX4 (Cat. No. 67763-1-Ig), GAPDH (Cat. No. 60004-1-Ig) and Lamin B (Cat. No. 12987-1-AP) were all from Proteintech (Chicago, IL, USA). The secondary antibodies for western blots, IRDye 800CW goat anti-mouse and goat anti-rabbit IgG (H+L) (Cat. No. 926-32210, Cat. No. 926-32211) were purchased from LI-COR Biosciences (Lincoln, NE, USA). Kits for the reverse transcription of RNA, PCR (Cat. No. 12574018), SYBR Green PCR (Cat. No. 4309155), siRNA sequence synthesis and co-immunoprecipitation assays (Cat. No. 26149) were acquired from Thermo Fisher Scientific (Waltham, MA, USA).

Serum biochemical assays and histopathological evaluation

Serum was centrifuged and tested according to the manufacturer's protocol and the final concentration was determined using a standard curve. Hematoxylin-eosin (HE) staining was performed on 5 µm paraffin thick sections. Representative pictures were obtained with a light microscope equipped with a digital camera (Leica Microsystems, Wetzlar, Germany). Six regions of three random sections were selected for evaluating the extent of necrosis, which was quantified using Image-Pro Plus 7.0 (Media Cybernetics, Rockville, MD, USA).

Measurement of MDA, GSH, and iron accumulation

Homogenized tissue and fragmented cell samples were prepared, and reaction reagents were added following the kit instructions. Using a standard curve as the control, the content of substances in cells or tissues was calculated for statistical analysis after correction for protein content.

ROS and lipid deposition determination

After warming frozen tissue sections to room temperature, 10 µM dihydroethidium (DHE) dye solution (λ excitation 510 nm, λ emission 590 nm) was added to cover the tissue and incubated for 60 m in a dark incubator at 37°C. After slightly drying the slices, 4',6'-diamidino-2-phenylindole (DAPI, λ excitation 350 nm, λ emission 420 nm) was added and incubated at room temperature in the dark for 10 m. Antifluorescence quenching sealing agent was used to seal and observe the sections. *In vitro*, treated adherent cells were incubated with 10 µM dihydroethidium diluted with serum-free culture medium for 30 m, and the cells were washed with serum-free culture medium three times to fully remove the staining solution that did not enter the cells. Fluorescence intensity was observed with a fluorescence microscope (Leica

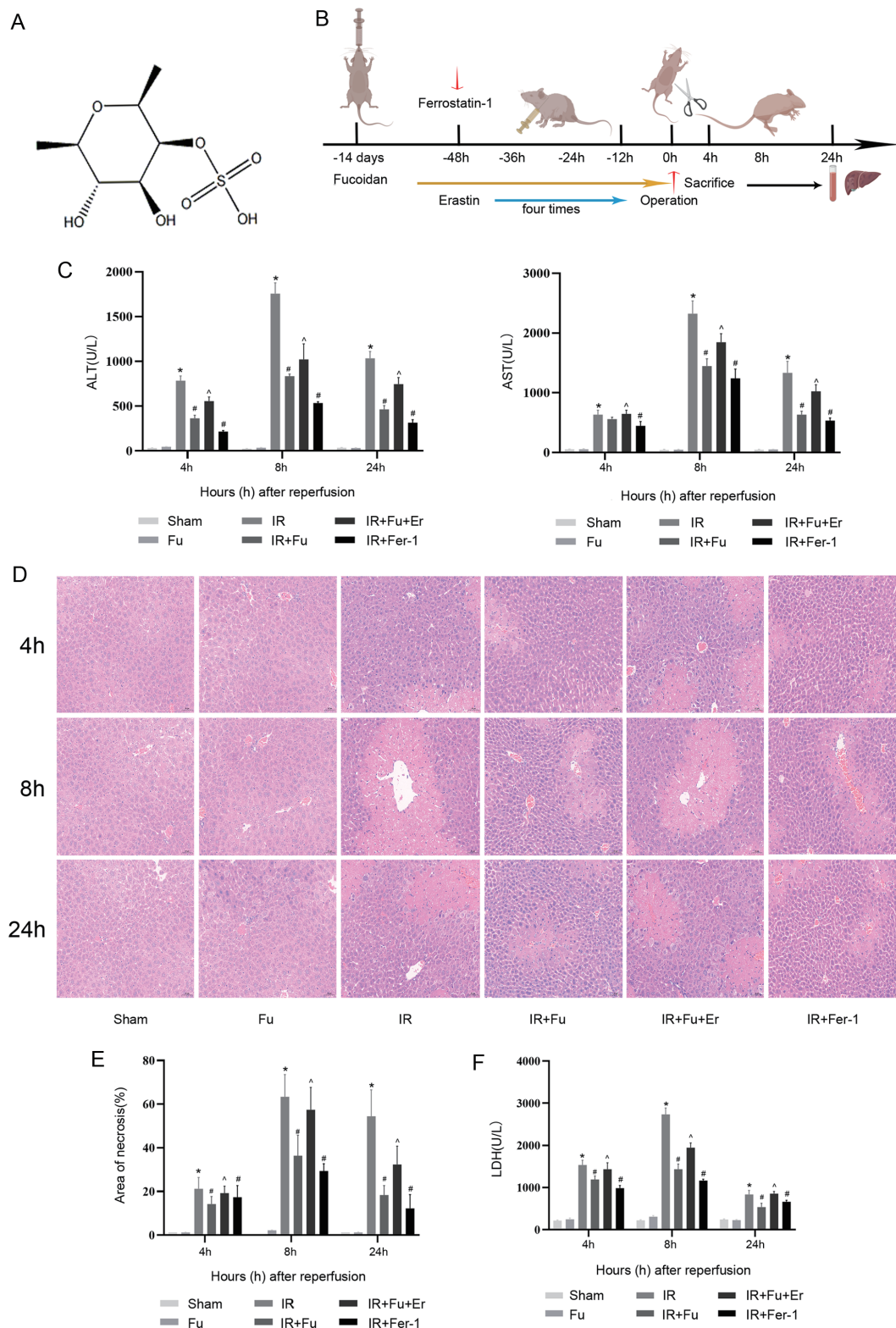


Fig. 1. Protective effect of fucoidan on IR-induced liver injury in mice. (A) Chemical structure of fucoidan. (B) Schematic diagram of the experimental procedures in mice. (C) Serum levels of ALT and AST. (D) Representative HE-stained liver sections shown by digital microscopy (200 \times). (E) Necrotic area stained with HE and analyzed with Image-Pro Plus 7.0. (F) Serum LDH ($n=6$). Data are means \pm SDs. * $p<0.05$ for IR vs. Sham, # $p<0.05$ for IR+fucoidan (Fu)/Fer-1 vs. IR, □ $p<0.05$ for IR+Fu+erastin (Er) vs. IR+Fu. ALT, Alanine transaminase; AST, Aspartate Transaminase; IR, Ischemia reperfusion; Er, Erastin; Fu, Fucoidan; Fer-1, Ferrostatin-1; LDH, Lactic dehydrogenase; HE, Hematoxylin-eosin staining.

Microsystems).

Oil red O dye solution was diluted with triple-distilled water at 3:2, passed through filter paper and placed at room temperature for 10 m to produce a wine-red solution without sedimentation. Frozen tissue sections were placed in the oil red O dye solution in the dark for 15 m, washed with triple-distilled water, and then put into the hematoxylin dye solution for 5 m. The sections were quickly differentiated in 1% hydrochloric acid and alcohol for 5 s, slowly washed with running water for 10 m, and observed directly. The red intensity of Reactive oxygen species (ROS) and the fat drop area ratio after oil red O dyeing were quantitatively analyzed by Image-Pro Plus 7.0.

Quantitative real-time polymerase chain reaction (qRT-PCR)

Total RNA from tissues and cells was extracted with TRIzol reagent (Invitrogen Corporation, Carlsbad, CA, USA) and then reverse transcribed into cDNA after quantitative and quality testing. The PCR reaction system was prepared according to the kit instructions by successively adding loading buffer, primers, dNTP mixture, Tag polymerase, and water to a total volume of 20 μ L. After a short centrifugation, gene expression was detected with a 7900HT fast real-time PCR system (Applied Biosystems, Foster City, CA, USA). Relative mRNA expression was calculated using $2^{-\Delta\Delta C_t}$ values and normalized to expression of glyceraldehyde-3-phosphate dehydrogenase (*GAPDH*). The primer sequences used in the experiment are shown in Table 1.

Western blot and co-immunoprecipitation assays

Total protein and nuclear protein from tissues and cells were extracted and quantified following the kit instructions. LO2 cells were incubated with 100 nm MG-132 for 1 h and then treated with fucoidan. The specific protein Nrf2 was isolated with ubiquitin by immunoprecipitation, and the isolated protein was resolved by electrophoresis. The prepared samples were electrophoresed through the separation gel, and when the bromophenol blue dye front had moved to the bottom of the gel, the gel was transferred to a polyvinylidene fluoride membrane. After blocking nonspecific sites with 5% nonfat milk powder for 1 h, primary antibodies were added, and the membrane was incubated with gentle shaking overnight at 4°C. The membranes were washed three times before the secondary antibody was added (dilution, 1:2,000) at room temperature for 1 h. The membranes were scanned with an Odyssey two-color infrared laser imaging system (LI-COR Biosciences) that determined the intensity of the protein bands.

Immunohistochemistry and immunofluorescence staining

Dewaxed paraffin sections were rehydrated by successive immersion in decreasing ethanol concentrations. The paraffin sections were then placed in a microwave oven for 10 m until the solution boiled. Endogenous catalase was blocked with 3% hydrogen peroxide. Bovine serum albumen (BSA) antigen blocking solution (5%) was prepared in 0.1% PBT with Tween (PBST) and incubated over the sections at room temperature for 60 min. Primary antibody diluted in 0.1% PBS was added and incubated overnight at 4°C, followed by addition of working solution for the second antibody from the corresponding species labeled with horseradish peroxidase and incubation at room temperature for 60 m. Diaminobenzidine condensed chromo reagent was added dropwise to the dried paraffin tissue, the color development was observed under the microscope, and the staining was terminated by

rinsing with tap water.

Treated-cell slides were fixed for 10 m, and after washing in PBS, 0.1% Triton X-100 in PBS was added for 10 m and the slides were then washed again with PBS. After blocking in 1% BSA, primary antibodies were added for overnight at 4°C. The following day, after washing with PBST three times, fluorescent second antibody was added in the dark for 1 h. Finally, an autofluorescence quenching sealing agent containing 4',6-diamidino-2-phenylindole (commonly known as DAPI) was used to seal the slides, which were then observed by a fluorescence microscope equipped with a digital camera.

Transmission electron microscopy

Fresh samples were placed immediately in fixing solution overnight at 4°C. The samples were then rinsed and incubated with 1% osmium tetroxide for 1 h. After dehydration through a series of diluted alcohols and treated with acetone, the resin was embedded overnight and replaced. Ultra-thin sections were prepared and photographed with an electron microscope (JEM-1230; JEOL Ltd, Tokyo, Japan) to show mitochondrial morphology.

Cell viability assay and siRNA transfection

Cells were placed in a 96-well plate at a density of 2×10^4 cells/mL and treated as described above for the cell model. After treatment, CCK-8 reagent was added and cell viability was obtained with a microplate reader (Synergy H4; BioTek, Winooski, VT, USA) with an excitation wavelength of 450 nm. For siRNA transfection, six-well plates were used to plate cells and 50 μ M siRNA-NC or siRNA-Nrf2 combined Lipofectamine 3000 was added to the cell culture for 8 h before HR according to the manufacturer's protocol. PCR and western blot analysis were used to determine the knockout effect. The sequences of effective siRNA-Nrf2 were sense 5'-GCCUGAAGUCCUGGUCAUTT-3', and antisense 5'-AUGACCAGGACUUACAGGCTT-3'.

Iron level and mitochondria detection

Living cells treated with drugs were removed from the cell culture medium, and Mito-Tracker Green working solution (λ excitation 505 nm, λ emission 535 nm) at a concentration of 50 nM was incubated with the cells at for 30 m at 37°C. After removing the liquid, serum-free culture medium containing 1 mM FerroOrange (λ excitation 543 nm, λ emission 580 nm) was added and the cells were observed directly after reacting at room temperature for 1 h. The red intensity of Fe^{2+} was quantitatively analyzed by Image-Pro Plus 7.0.

RNA sequencing

Fresh liver tissue from the IR and fucoidan groups ($n=3$) was prepared as described for standardized sample processing and sent to the Shanghai Yanjiang Biotechnology Co., Ltd. (Shanghai, China) for high-throughput sequencing using an Illumina Hiseq sequencing platform. The pretreated data were subjected to quality control by FastQC software and then analyzed for differentially expressed genes (DEGs). If the fold-change was ≥ 2 and the corresponding corrected p -value was < 0.05 , the gene was considered to be differentially expressed. The Sangerbox tool (<http://vip.sangerbox.com/home.html>) was used to complete gene ontology (GO) and Kyoto Encyclopedia of Genes and Genomes (KEGG) analysis to determine functional annotation and pathway enrichment. A heat map was used to display gene expression, and Venn maps were drawn to obtain the intersection of up-regulated genes in liver tissues and inhibitory genes from FerrDb (<http://www.zhounan.org/ferrdb>).²⁷

Table 1. Nucleotide sequences of primers used for qRT-PCR

Species	Gene		Primer sequence (5'-3')
Mouse	NRF2	Forward	ACCAAGGGGCACCATATAAAAG
		Reverse	CTTCGCCGAGTTGCACTCA
	HO-1	Forward	CCTCGGACAAACTGGCACT
		Reverse	CCGACGCCTGACAACATCT
	GPX4	Forward	TGTGCATCCC CGCATGATT
		Reverse	CCCTGTACTTATCCAGGCAGA
	GCH1	Forward	GCCGCTTACTCGTCCATTCT
		Reverse	GAACAAGGTGATGCTCACACA
	FTH1	Forward	CAAGTGCGCCAGAACTACCA
		Reverse	ACAGATAGACGTAGGAGGCATAC
	TFAP2A	Forward	ACGACCCCTACAGCCTGAAT
		Reverse	GCGTGTAGGTAAGGAGTGG
	SREBF1	Forward	TGACCCGGCTATTCCGTGA
		Reverse	CTGGGCTGAGCAATACAGTTC
	SQSTM1	Forward	GAGGCACCCCGAAACATGG
		Reverse	ACTTATAGCGAGTTCCACCA
	FANCD2	Forward	CAAATCAGCTAGGTGTGGATCA
		Reverse	CCAGGCCATTAACAACTCTTCT
	TFRC	Forward	GTTTCTGCCAGCCCTTATTAT
		Reverse	GCAAGGAAAGGATATGCAGCA
	PRKAA2	Forward	AAGATCGGACACTACGTCTCTG
		Reverse	TGCCACTTTATGGCCTGTCAA
	ATF4	Forward	CCTGAACAGCGAAGTGTGG
		Reverse	TGGAGAACCCATGAGGTTTCAA
GAPDH	Forward	AATGGATTTGGACGCATTGGT	
	Reverse	TTTGCCTGGTACGTGTTGAT	
Human	NRF2	Forward	GGCGTTAGAAAGCATCCTTCC
		Reverse	GCAGAGGGCACACTCAAAGT
	HO-1	Forward	CTGTGCCACCTGGAAGTAC
		Reverse	TCTTGTGGGTCTTGAGCTGTT
	GPX4	Forward	GAGGCAAGACCGAAGTAAACTAC
		Reverse	CCGAACTGGTTACACGGGAA
	GAPDH	Forward	TGTGGGCATCAATGGATTTGG
		Reverse	ACACCATGTATTCCGGGTCAAT

NRF2, Nuclear factor erythroid related factor 2; HO-1, Heme oxygenase 1; GPX4, Glutathione Peroxidase 4; GCH1, GTP cyclohydrolase 1; FTH1, Ferritin heavy polypeptide 1; TFAP2A, Transcription Factor AP-2 alpha; SREBF1, Sterol Regulatory Element Binding Transcription Factor 1; SQSTM1, Sequestosome 1; FANCD2, Fanconi anemia, complementation group D2; TFRC, Transferrin receptor; PRKAA2, Protein kinase AMP-activated alpha-2; ATF4, Activating Transcription Factor 4; GAPDH, glyceraldehyde-3-phosphate dehydrogenase.

Statistical analysis

Results were reported as means±SDs and analyzed with SPSS 22.0 (IBM Corp., Armonk, NY, USA). The overall significance of data was determined through one-way analysis of variance with the Bonferroni correction for comparisons between groups. A *p*-value of <0.05 was considered statistically significant. Positively stained areas in this study were evaluated with Image-Pro Plus 7.0.

Results

Fucoidan protects against IR-induced liver injury by inhibiting ferroptosis

Fucoidan is an anionic sulfated polysaccharide with a molecular formula of C₇H₁₄O₇S extracted from marine brown algae. The chemical structure shown in Figure 1A. Beginning 2 weeks before the IR operation, we administered fucoidan to

mice at 40 mg/kg by gavage and injected erastin and Fer-1 as ferroptosis regulators to observe the extent of liver injury after IR (Fig. 1B). The results showed that the group receiving fucoidan alone had no obvious toxic or side effects in the liver at each time point from 4 to 24 h. The IR group had significant increases of ALT and AST, indicating that a model of IR injury had been successfully established. In addition, compared with the IR group, the liver enzyme levels of the fucoidan pretreatment group decreased significantly, similar to effect of Fer-1, while the ferroptosis inducer erastin reversed the suppressive effects of fucoidan on liver enzymes, most prominently at 8 h (Fig. 1C). Based on the pathological evaluation of HE staining in liver tissue, and consistent with the level of liver enzymes, the IR group exhibited cytoplasmic concentration and cell structure disorders 4 h after IR surgery. Fusion lamellar necrosis, nuclear pyknosis, and fragmentation began to appear at 8 h. In the fucoidan and Fer-1 treatment groups, necrosis was significantly reduced, but necrosis worsened after treatment with erastin. The change in necrotic area was statistically significant in erastin-treated animals (Fig. 1D, E). The serum LDH level also indicated ongoing cell necrosis. It was present at each time point, but the LDH level was significantly increased in the IR group, while treatment with fucoidan, and Fer-1 decreased the LDH level. Similarly, erastin significantly reversed the decrease in LDH produced by fucoidan or Fer-1 (Fig. 1F). The above results suggest that IR-induced liver injury was related to ferroptosis and ferroptosis inhibitors effectively protected liver function.

Fucoidan inhibits oxidative stress and lipid peroxidation

To further verify the inhibitory effect of fucoidan on ferroptosis, we evaluated the level of cellular oxidative stress products when the effect was most obvious at 8 h. Initially, the application of fucoidan alone in tissues did not cause significant changes in the accumulation of MDA, GSH, or iron, but IR significantly increased the accumulation of MDA and iron in cells and decreased GSH. Conversely, fucoidan treatment significantly inhibited the production of MDA and iron and promoted GSH to play a positive role (Fig. 2A). We used DHE and oil red O to stain frozen liver tissue to more clearly show ROS and lipid peroxidation levels in liver cells. The results showed that the fluorescent DHE staining in the IR group was significantly enhanced, and the area of positive oil red O staining increased, but staining decreased after fucoidan treatment (Fig. 2B, C). The results show that fucoidan effectively eliminated IR-induced iron accumulation, oxidative stress products and inhibited lipid peroxidation *in vivo*, and may be an effective inhibitor of ferroptosis.

Fucoidan regulates ferroptosis mediated by the Nrf2/HO-1/GPX4 axis

Bioinformatics analysis found 1887 DEGs after IR and fucoidan treatment, of which 1208 were up-regulated and 679 were down-regulated (Fig. 3A, B). GO functional annotation showed the biological process of DEG enrichment in programmed cell death, and the analysis of KEGG pathway enrichment found DEGs focused on the ferroptosis pathway (Fig. 3D). A total of 12 common genes were screened by FerrDb between the 1208 up-regulated DEGs and the 237 suppressor genes (Fig. 3C). To further confirm the relationship between fucoidan and ferroptosis, we screened the key pathway molecules of ferroptosis in the IR and fucoidan pretreatment groups, and found that Nrf2, HO-1, and GPX4, which are most closely related to oxidative stress, had the most significant changes (Fig. 3E).

Fucoidan inhibits ferroptosis through the Nrf2/HO-1/GPX4 pathway in vivo

We also verified the expression of the above genes in all groups. The genes decreased significantly in the IR group but increased significantly in the fucoidan pretreatment group (Fig. 4A). We extracted tissue protein for verification and found that the total protein level of the three above factors was significantly inhibited by IR, but the expression of Nrf2 increased in the fucoidan pretreatment group. However, Nrf2 mainly exerts its effect in the nucleus. We therefore isolated nuclear protein from cells for verification and found that the level of Nrf2 in the nucleus was consistent with that of total protein and its expression intensity relative to the internal reference gene was quantitatively counted (Fig. 4B). We then used immunohistochemical methods to visualize protein expression. We observed in liver tissue that the expression of Nrf2 and GPX4 in the fucoidan single-drug group was consistent with the control group but the induction of IR significantly inhibited the increase in Nrf2 and GPX4. After treatment of IR-injured animals with fucoidan, the proportion of Nrf2 in the nucleus increased, and GPX4 increased uniformly. Mitochondrial morphology observed by electron microscope is also an important sign of ferroptosis. We found that mitochondria in the IR group were significantly smaller, membrane density was increased, cristae were reduced or even absent, but morphological changes in the fucoidan-treated group were significantly improved (Fig. 4C). The results suggest that the mechanism by which fucoidan inhibited ferroptosis was related to the Nrf2/HO-1/GPX4 pathway, which is closely related to oxidative stress.

Fucoidan protects against hepatocyte injury induced by HR

In vitro, we simulated the *in vivo* IR model (C-IR) by HR, and used erastin and Fer-1 as regulators of ferroptosis. First, we tested cell survival with cell counting kit-8 (CCK-8) assays and found that at the same time point, the cell death rate in the IR model group increased, but treatment with fucoidan and Fer-1 partially maintained the survival of hepatocytes. Erastin reversed the protective effect of fucoidan, and the effect was most significant after 24 h, but the high death rate in the 48 h model group was not suitable for the study time point (Fig. 5A). Similarly, the levels of MDA, GSH, and LDH in cells are important markers of oxidative stress. Similar to the *in vivo* results, the levels of MDA and LDH increased and GSH levels decreased in a HR-dependent manner, which was reversed by fucoidan and Fer-1 treatment, whereas erastin exerted an effect consistent with induced *in vivo* injury (Fig. 5B). The level of lipid peroxidation in cells was also shown by the presence of red lipid droplets stained by oil red O, and their presence was consistent with increased concentrations of ROS and iron (Fig. 5C). The above fluorescence intensity and areas with red fat droplets differed significantly between the groups (Fig. 5D). In addition, we verified the protein level of related molecules in the pathway by western blot assays, which showed that Nrf2, HO-1, and GPX4 levels in both the cytosol and nucleus were significantly down-regulated by HR, but increased again after treatment with fucoidan and Fer-1. Erastin reversed that effect, which was significantly correlated with the ferroptosis level. The relative strength of the protein bands was quantified, and the results indicated that fucoidan protected hepatocytes from hypoxia and reoxygenation *in vitro*.

Fucoidan protects hepatocytes by inhibiting Nrf2/HO-1/GPX4 axis-mediated ferroptosis

To further verify the role of Nrf2 as the key link in ferropto-

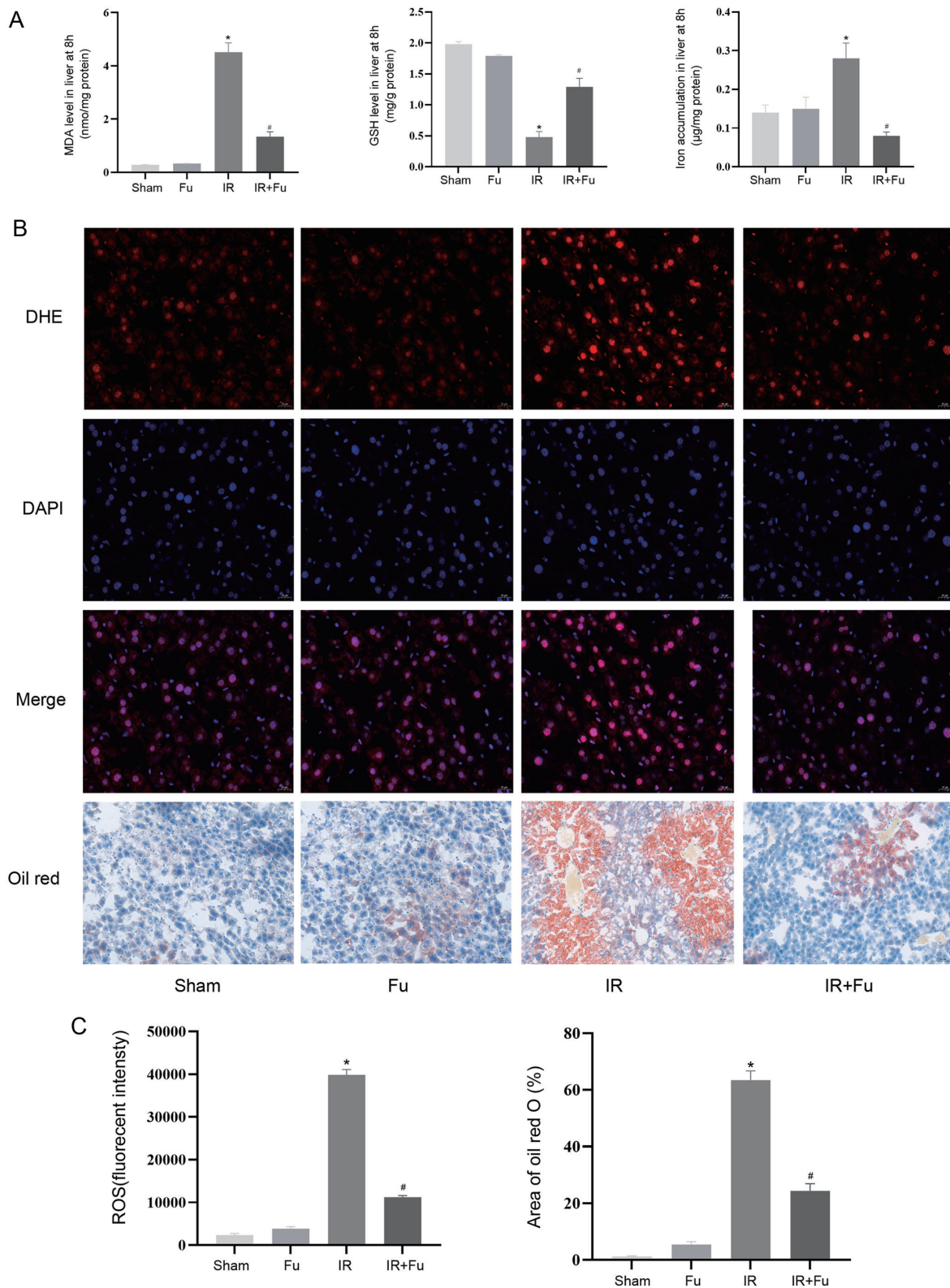


Fig. 2. Effect of fucoïdan on oxidative stress and lipid peroxidation in mice. (A) MDA, GSH, and iron accumulation in liver tissue. (B) ROS and lipid accumulation were detected by DHE (200×) and oil red O (400×), respectively. (C) Fluorescence intensity of ROS and the area of oil red O staining analyzed with Image-Pro Plus 7.0 ($n=6$). Data are means±SDs. * $p<0.05$ for IR vs. Sham, # $p<0.05$ for IR+fucoïdan (Fu) vs. IR. MDA, Malonaldehyde; GSH, L-Glutathione; ROS, Reactive oxygen species; DHE, Dihydroethidium; IR, Ischemia reperfusion; Fu, Fucoïdan.

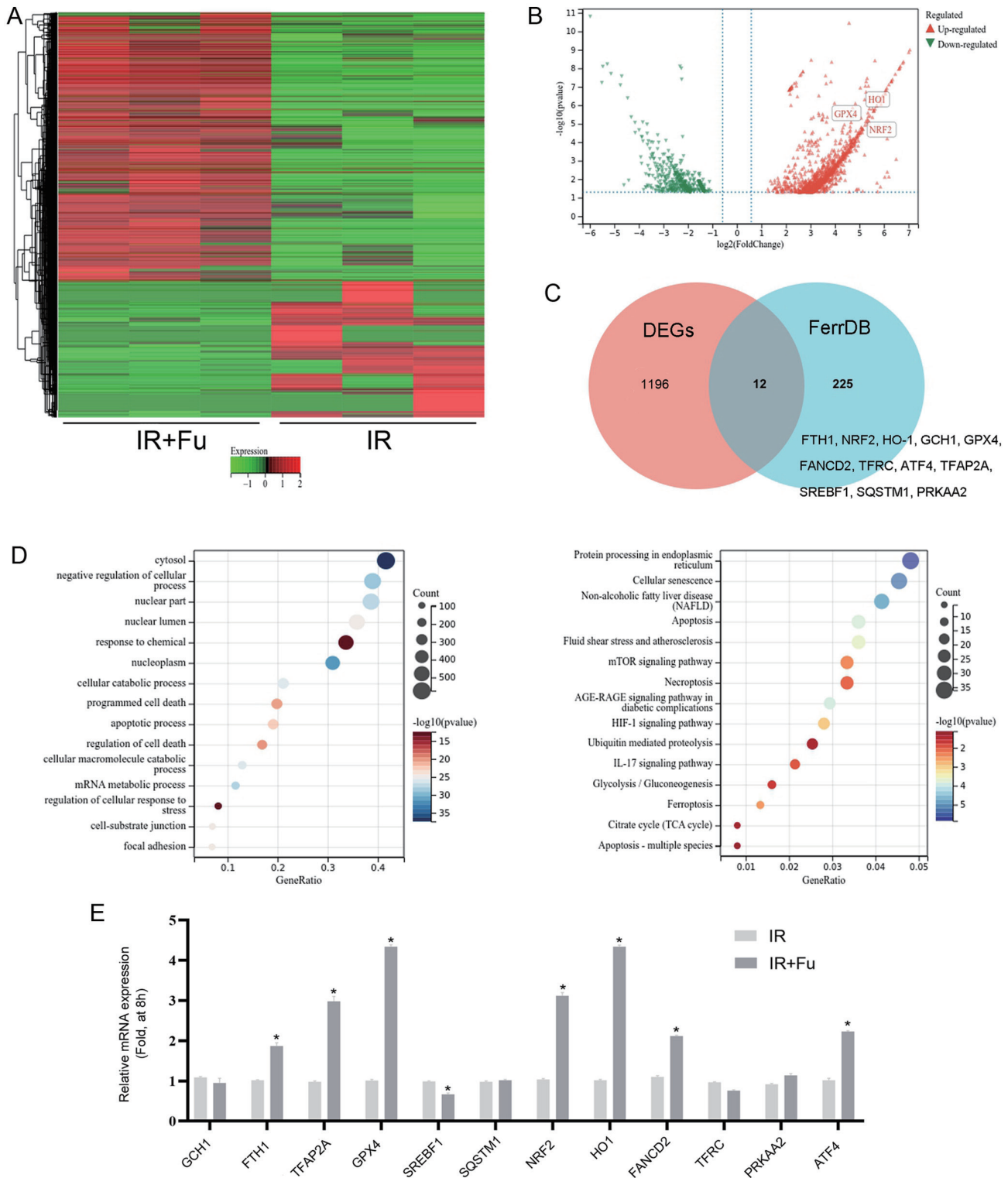


Fig. 3. Bioinformatics analysis of the fucoidan action mechanism. (A) Heatmap of DEGs. (B) Volcano map of DEGs. (C) Venn diagram of DEGs and suppressor genes from FerrDb. (D) GO and KEGG annotation and enrichment analysis. (E) mRNA expression of ferroptosis-related genes in the liver was detected by real-time quantitative PCR ($n=6$). Data are means \pm SDs. * $p < 0.05$ for IR+fucoidan (Fu) vs. IR. NRF2, Nuclear factor erythroid 2-related factor 2; HO-1, Heme oxygenase 1; GPX4, Glutathione Peroxidase 4; GCH1, GTP cyclohydrolase 1; FTH1, Ferritin heavy polypeptide 1; TFAP2A, Transcription Factor AP-2 alpha; SREBF1, Sterol Regulatory Element Binding Transcription Factor 1; SQSTM1, Sequestosome 1; FANCD2, Fanconi anemia, complementation group D2; TFRC, Transferrin receptor; PRKAA2, Protein kinase AMP-activated alpha-2; ATF4, Activating Transcription Factor 4; GAPDH, glyceraldehyde-3-phosphate dehydrogenase; IR, Ischemia reperfusion; Fu, Fucoidan; DEGs, Differentially expressed genes; PCR, Polymerase chain reaction.

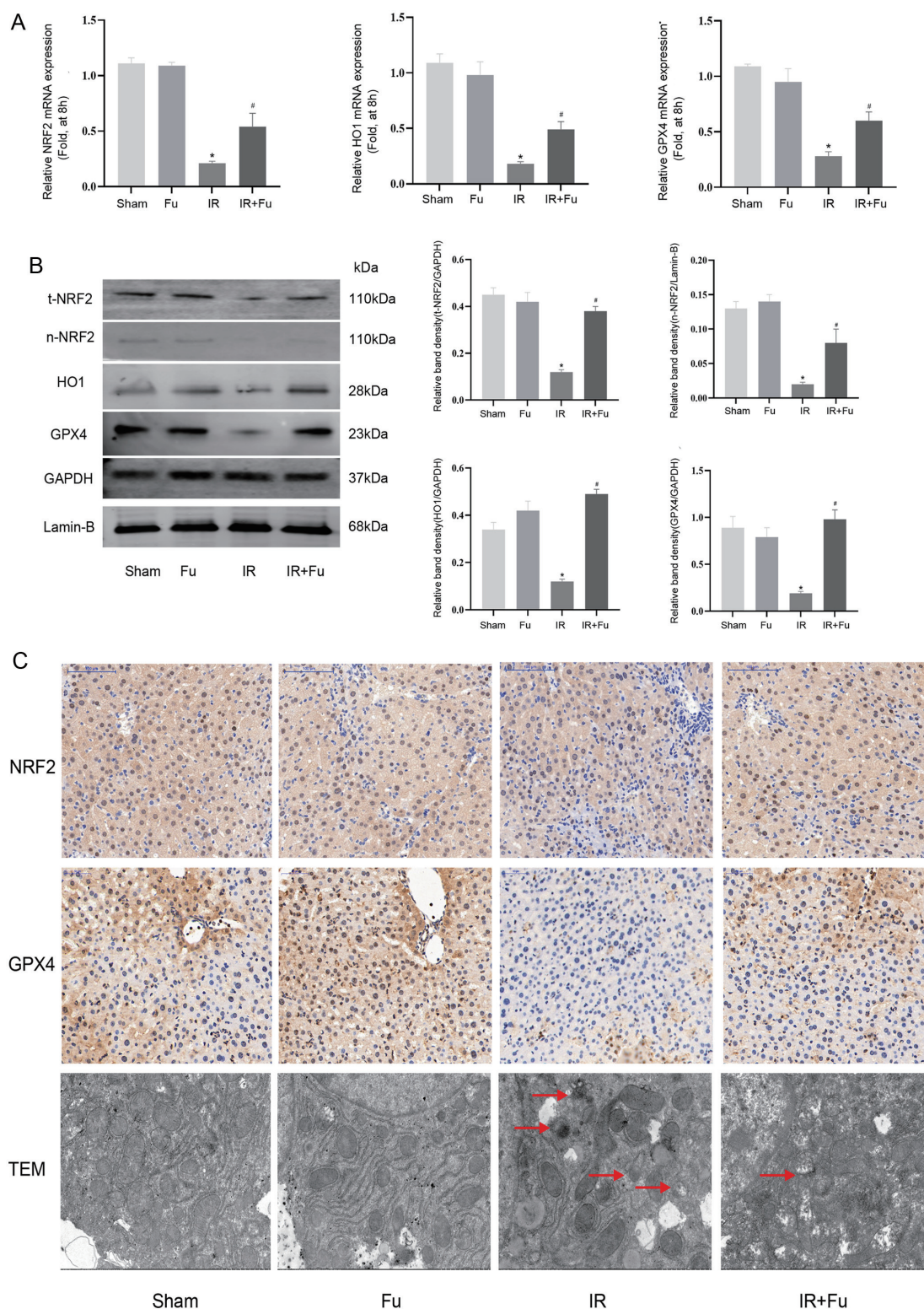


Fig. 4. Effect of fucoxanthin on the Nrf2/HO-1/GPX4 pathway in mice. (A) mRNA expression of Nrf2, HO-1, and GPX4 by real-time quantitative PCR. (B) Protein expression of total-Nrf2, nuclear-Nrf2, HO-1, and GPX4 shown in western blots. Band density relative to housekeeping genes was analyzed with Image-Pro Plus 7.0. (C) Representative images of liver tissue with immunohistochemical staining of Nrf2 and GPX4. Transmission electron microscopy was used to detect the mitochondrial morphology during ferroptosis in liver tissue. Red arrows show damaged mitochondria (4,000 \times ; $n=6$). Data are means \pm SDs. * $p<0.05$ for IR vs. Sham, # $p<0.05$ for IR+fucoxanthin (Fu) vs. IR. Nrf2, Nuclear factor erythroid 2-related factor 2; HO-1, Heme oxygenase 1; GPX4, Glutathione Peroxidase 4; GAPDH, glyceraldehyde-3-phosphate dehydrogenase; TEM, Transmission electron microscope.

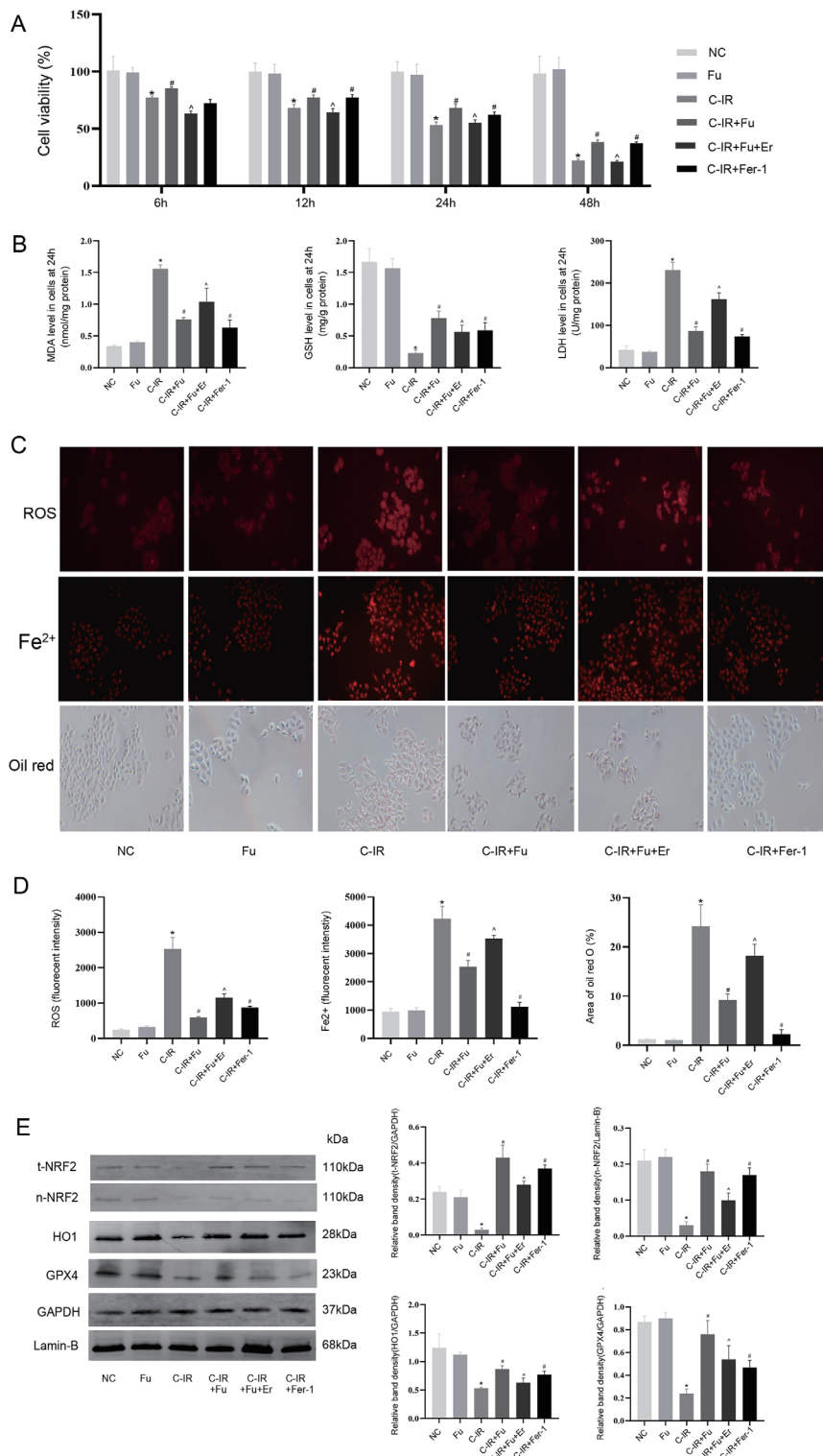


Fig. 5. Protective effect of fucoidan against HR-induced hepatocyte injury in vitro. (A) LO2 cells were treated with fucoidan for 6–48 h. CCK8 kits were used to monitor cell viability. (B) MDA, GSH, and LDH content in liver cells. (C) ROS, Fe²⁺ and lipid accumulation levels detected by DHE, Ferro Orange (200×) and oil red O (400×), respectively. (D) Fluorescence intensity of ROS, Fe²⁺ and the area of oil red O staining were analyzed with Image-Pro Plus 7.0. (E) Protein expression of total-Nrf2, nuclear-Nrf2, HO-1, and GPX4 was determined in western blots. Relative band density to housekeeping genes was analyzed with Image-Pro Plus 7.0 (*n*=6). Data are means±SDs. **p*<0.05 for C-IR vs. Sham, #*p*<0.05 for C-IR+fucoidan (Fu)/Er-1 vs. C-IR, □*p*<0.05 for C-IR+Fu+erastin (Er) vs. C-IR+Fu. MDA, Malonaldehyde; GSH, L-Glutathione; ROS, Reactive oxygen species; DHE, Dihydroethidium; IR, Ischemia reperfusion; Fu, Fucoidan; LDH, Lactic dehydrogenase; DHE, Dihydroethidium; Nrf2, Nuclear factor erythroid 2-related factor 2; HO-1, Heme oxygenase 1; GPX4, Glutathione Peroxidase 4; GAPDH, Glyceraldehyde-3-phosphate dehydrogenase; Er, Erastin; Fer-1, Ferrostatin-1.

sis, we synthesized siRNA to knock out Nrf2, and demonstrated that siRNA-Nrf2-2 had the best effect in regulating Nrf2-2 RNA (Fig. 6A). We then modeled the cells and treated them with fucoïdan, followed by down-regulation of Nrf2 to verify the causal relationship between the drugs and the pathways. First, we double-stained intracellular iron and mitochondria and found that fucoïdan significantly reduced the increase in iron induced by HR. Down-regulation of Nrf2 by siRNA reversed the effect of fucoïdan, which was correlated with changes in mitochondria (Fig. 6B, C). The PCR results and protein levels of Nrf2, HO-1, and GPX4 also demonstrated that fucoïdan simultaneously increased the gene and protein expression of these factors, and that down-regulating Nrf2 significantly weakened the protective effect of fucoïdan, shown by quantitation of protein level intensity (Fig. 6D, E). To more clearly show changes in the expression of related molecules in the cell, we used cellular immunofluorescence to verify that hypoxia and reoxygenation significantly reduced the expression of Nrf2, and that fucoïdan promoted the entry of Nrf2 into the nucleus. After down-regulation of Nrf2, its expression and rate of entry into the nucleus were significantly decreased. Similarly, the fluorescence intensity of GPX4 was weakened in the model group and was inhibited by siRNA-Nrf2 after being increased by fucoïdan (Fig. 6G). Finally, increased ubiquitination and Nrf2 binding in LO2 cells in the model group were reduced by fucoïdan, which further confirmed the molecular mechanism of fucoïdan acted via Nrf2 (Fig. 6F). The results suggest that fucoïdan acted to protect against hepatocyte injury induced by HR by inhibiting ferroptosis mediated by the Nrf2/HO-1/GPX4 pathway.

Discussion

At present, treatments are mainly intended to improve the metabolism of ischemic tissue, antioxidation, scavenging of free radicals, and other measures to mobilize endogenous adaptive protective mechanisms.³ In this study, we confirmed that ferroptosis occurred during of IR, and that fucoïdan can inhibit iron accumulation in hepatocytes through the Nrf2/HO-1/GPX4 pathway. Thus, fucoïdan was an effective inhibitor of ferroptosis, and is a potential drug to prevent IR injury.

Fucoïdan is extracted from brown algae and some marine invertebrates. It has a wide range of applications in medicine, food, and industry owing to its antioxidant, antitumor, and other biological activities.¹³ Recent advances in extraction and preparation have overcome difficulties in mass production and have expanding its range of uses.²⁸ Toxicological studies of fucoïdan have shown that there are no significant adverse reactions in humans and mice at higher doses.^{19,29} We first divided mice into groups and carried out pretreatment with fucoïdan in a mouse model of IR injury similar to liver transplantation. In those experiments, we used Fer-1 as a positive control. Erastin simulated the occurrence of ferroptosis. The results showed that fucoïdan and Fer-1 significantly reduced the levels of serum ALT, AST, and LDH, and reduced the size of necrotic areas as shown in pathological sections, and erastin reversed the effect of fucoïdan and damaged liver cells. The above effects were most significant after 8 h of treatment. This shows that inhibition of ferroptosis had a protective role in the liver. Fucoïdan had the same protective effect as the inhibitor Fer-1, but its mechanism needs to be further clarified.

Sufficient evidence has been produced showing that ROS accumulation and lipid peroxidation occur in the process of IR injury, accompanied by the production of MDA and the

consumption of GSH, and these factors are closely related to ferroptosis.^{30,31} In this study, we further examined the groups related to drug treatment at 8 h to detect the level of liver oxidative stress. It was found that the increase of MDA and decrease of GSH induced by IR were significantly improved by fucoïdan supplementation, and the visual ROS level and lipid droplets stained by oil red O were also correspondingly reduced. The large amount of iron accumulated in the process was also down-regulated by fucoïdan, which was in a stable state. Therefore, we have reason to further speculate that fucoïdan eliminated harmful ROS and inhibited lipid peroxidation in the process, and also inhibited ferroptosis by regulating the level of iron, thus significantly improving cell function.

Studies of the regulation of iron death are currently focused on the metabolism of System Xc-, GSH metabolism, GPX4 activity, and ROS production. There are many related molecules, including fms-related tyrosine kinase 1 (FLT1), FTH1, GPX4, fibroblast Specific Protein 1 (FSP1), solute Carrier Family 7 Member 11 (SLC7A11), Nrf2, TFRC, acyl-CoA synthetase long-chain family member 4 (ACSL4), and others.³²⁻³⁶ Both Xu *et al.*³⁷ and Qi *et al.*³⁸ confirmed that brown rice extracts improved lipid peroxidation, cytotoxicity, and delayed proliferation induced by GPX4 knockdown, and that dimethyl fumarate protected the liver from IR injury by reducing ferroptosis mediated by Nrf2 and SLC7A11. To confirm the specific action pathway of fucoïdan, we performed RNA sequencing and biological information analysis of liver tissue to screen for the major molecular players and found that changes in the expression of Nrf2, HO-1, and GPX4 closely related to GSH metabolism were the most significant. Multiple validation by PCR, western blotting, and immunohistochemical staining confirmed that IR inhibited the transcription and expression of the above genes in mice, by inhibiting the entry of Nrf2 into the nucleus, and that fucoïdan treatment reversed the above changes. Fucoïdan pretreatment also lessened the mitochondrial changes caused by IR, including the reduction of mitochondrial cristae, rupture of the outer membrane, and shrinkage of mitochondria. Based on the above results, when IR-induced cells produce a large amount of lipid ROS, the GSH antioxidant system is activated, ubiquitinated Nrf2 entry into the nucleus is inhibited, and HO-1 and GPX4 are reduced, resulting in ferroptosis. Fucoïdan promoted Nrf2 entry into the nucleus and transcription of HO-1 and GPX4 by clearing a large number of ROS products, thus directly inhibiting ferroptosis.³⁹

Because of factors interfering with the *in vivo* experiment, we explored the mechanism *in vitro*. First, we established a hepatocyte model of hypoxia and reoxygenation. Similar to the *in vivo* experiments, we used ferroptosis regulators and fucoïdan to treat cells synchronously and found that fucoïdan protected against hepatocyte death, which is consistent with the effect of Fer-1. Fucoïdan also reversed the increase in MDA, LDH, and GSH induced by IR and erastin, and was aided in the removal of ROS by inhibiting iron involvement and lipid droplet formation. Overall, the results indicate that in isolated hepatocytes, the antioxidant activity of fucoïdan and regulation of iron homeostasis were prominent. The preliminarily verified pathway molecules also showed that fucoïdan reduced the rates of ubiquitin and Nrf2 binding and promoted the entry of Nrf2 into the nucleus, resulting in increased expression of HO-1 and GPX4, which also inhibited ferroptosis. After knockout of Nrf2, fucoïdan was no longer protective, resulting in serious damage to mitochondria, iron accumulation in cells, and simultaneous damage to liver function, suggesting that the Nrf2/HO-1/GPX4 axis played a key role

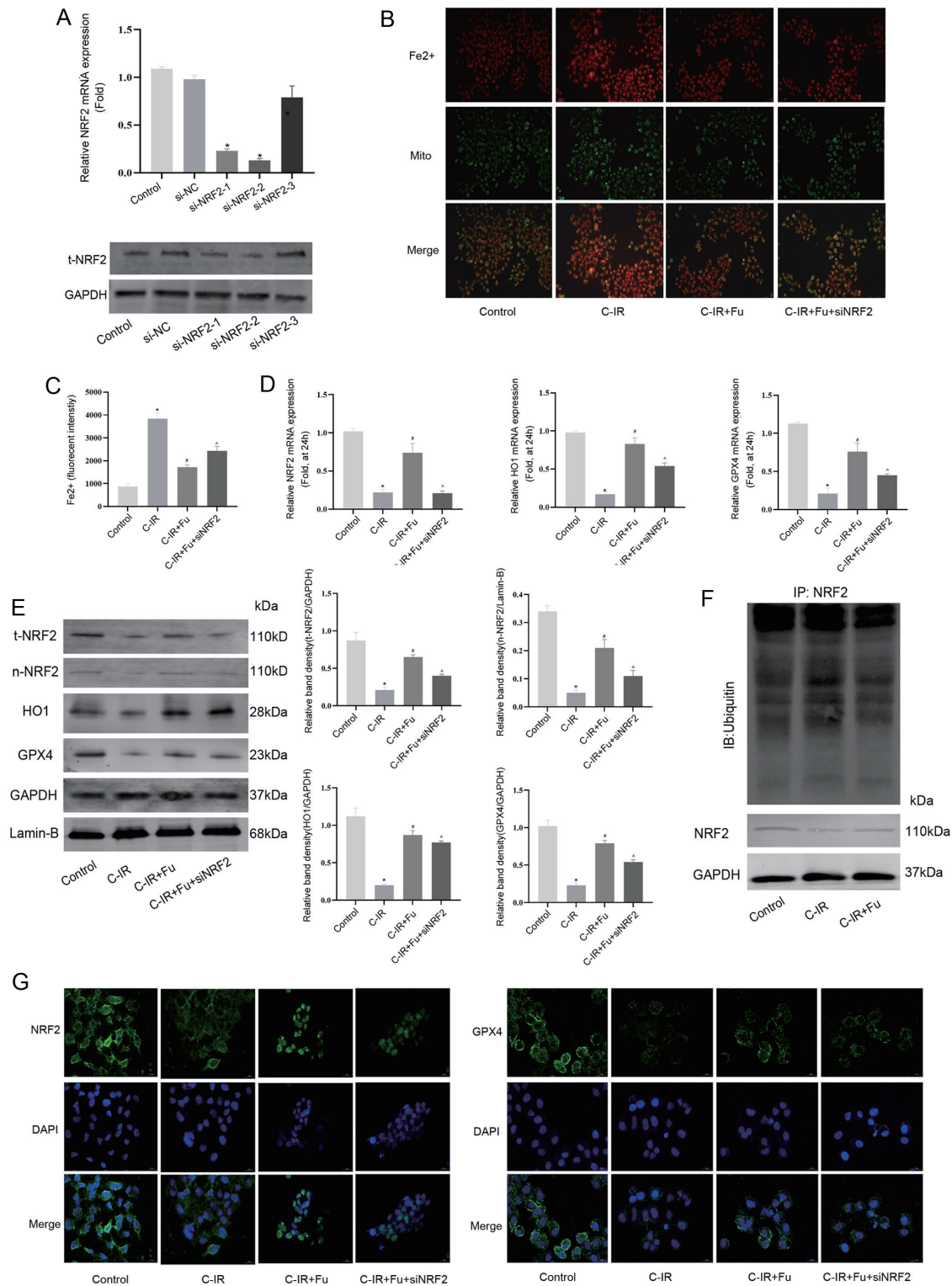


Fig. 6. Effect of fucoidan on the Nrf2/HO-1/GPX4 axis *in vitro*. (A) mRNA and protein expression of Nrf2 detected by real-time quantitative PCR and western blots, respectively. (B) Levels of Fe²⁺ and mitochondrial localization detected by Ferro Orange and Mito Green (200×). (C) Fe²⁺ fluorescence intensity analyzed with Image-Pro Plus 7.0. (D) mRNA expression of Nrf2, HO-1, and GPX4 detected by real-time quantitative PCR. (E) Protein expression of total-Nrf2, nuclear-Nrf2, HO-1, and GPX4 determined by western blots. Relative band density to housekeeping genes was analyzed with Image-Pro Plus 7.0. (F) Ubiquitination of Nrf2 protein in LO2 cells. (G) Subcellular localization of Nrf2 and GPX4 expression in LO2 cells shown by immunofluorescence staining (400×; (n=6). Data are means±SDs. **p*<0.05 for C-IR vs. control, #*p*<0.05 for C-IR+fucoidan (Fu) vs. C-IR, □*p*<0.05 for C-IR+Fu+siNRF2 vs. C-IR+Fu. Nrf2, Nuclear factor erythroid 2-related factor 2; HO-1, Heme oxygenase 1; GPX4, Glutathione Peroxidase 4; GAPDH, glyceraldehyde-3-phosphate dehydrogenase; DHE, Dihydroethidium; IR, Ischemia reperfusion; Fu, Fucoidan; PCR, Polymerase chain reaction.

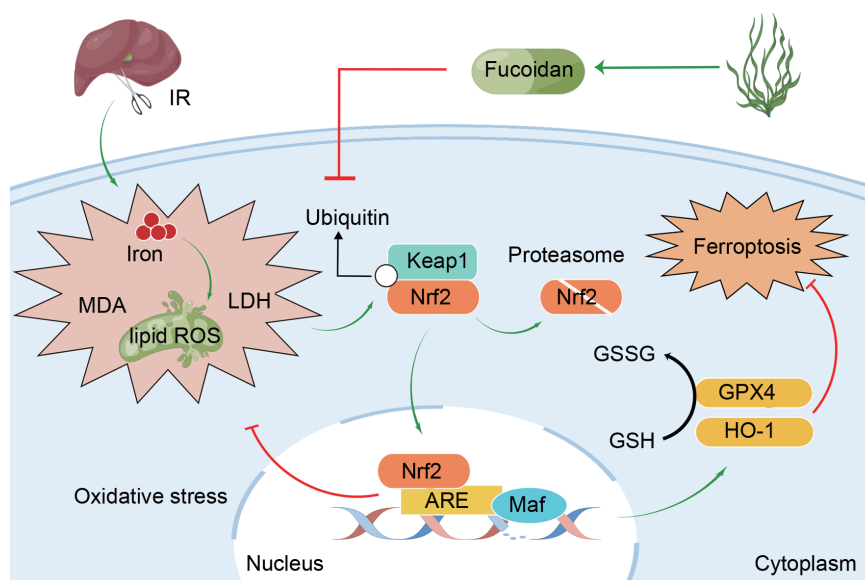


Fig. 7. Mechanism of fucoidan action on ferroptosis via the Nrf2/HO-1/GPX4 axis. In the liver, ischemia and reperfusion are accompanied by accumulation of iron and lipid peroxidation-induced ROS accumulate in hepatocytes and mitochondria to induce ferroptosis that damages hepatocytes. Fucoidan pretreatment reduced Nrf2 ubiquitination, promoted Nrf2 entry into the nucleus, and increased transcription of HO-1 and GPX4 to protect liver cells from injury by inhibiting ferroptosis. MDA, Malonaldehyde; GSH, L-Glutathione; GSSG, L-Glutathione Oxidized; ROS, Reactive oxygen species; IR, Ischemia reperfusion; LDH, Lactic dehydrogenase; DHE, Dihydroethidium; Nrf2, Nuclear factor erythroid 2-related factor 2; HO-1, Heme oxygenase 1; GPX4, Glutathione Peroxidase 4.

in HR-induced liver cell, ferroptosis consistent with the *in vivo* results (Fig. 7).

Conclusions

In conclusion, we demonstrated that ferroptosis was involved in the pathophysiology of IR injury, characterized by excessive ROS production and lipid peroxidation. Fucoidan had an important role in inhibiting ferroptosis and restoring iron homeostasis by Nrf2/HO-1/GPX4. In future clinical practice, it may be used as a drug target to screen for more efficient and safe antioxidant drugs for the treatment of IR injury.

Funding

This study was supported by the National Natural Science Foundation of China (No. 82100638; 81772591), Shanghai Municipal Commission of Health and Family Planning (No. 201740156) and the Shanghai Sailing Program (No. 20YF1443300).

Conflict of interest

The authors have no conflict of interests related to this publication.

Author contributions

Study concept and design (CYG, XFX), acquisition of data (JJL, WQD, WHM), analysis of data (YYL, WQX, JJL), drafting of the manuscript (JJL, WQD), and material support and study supervision (WQX, CYG, JJL, WQD).

Ethical statement

All animal experiments were performed according to the National Institutes of Health (USA) Guidelines for the Care and Use of Laboratory Animals. The experiment protocol was

conducted according to the Declaration of Helsinki with the approval of the Shidong Hospital Research Ethics Committee (No. 2020-0002).

Data sharing statement

No additional data are available.

References

- [1] Muhammad H, Tehreem A, Ting PS, Gurakar M, Li SY, Simsek C, *et al*. Hepatocellular Carcinoma and the Role of Liver Transplantation: A Review. *J Clin Transl Hepatol* 2021;9(5):738–748. doi:10.14218/JCTH.2021.00125, PMID:34722189.
- [2] Thorgersen EB, Barratt-Due A, Haugaa H, Harboe M, Pischke SE, Nilsson PH, *et al*. The Role of Complement in Liver Injury, Regeneration, and Transplantation. *Hepatology* 2019;70(2):725–736. doi:10.1002/hep.30508, PMID:30653682.
- [3] Xu X. State of the art and perspectives in liver transplantation. *Hepatobiliary Pancreat Dis Int* 2023;22(1):1–3. doi:10.1016/j.hbpd.2022.12.001, PMID:36528548.
- [4] Zhang Y, Huang C, Ju W, Zhao Q, Chen M, Wang L, *et al*. Avoiding Ischemia Reperfusion Injury in Liver Transplantation. *J Vis Exp* 2020;(166):e61485. doi:10.3791/61485, PMID:33346199.
- [5] Wang H, Xi Z, Deng L, Pan Y, He K, Xia Q. Macrophage Polarization and Liver Ischemia-Reperfusion Injury. *Int J Med Sci* 2021;18(5):1104–1113. doi:10.7150/ijms.52691, PMID:33526969.
- [6] Chen X, Li J, Kang R, Klionsky DJ, Tang D. Ferroptosis: machinery and regulation. *Autophagy* 2021;17(9):2054–2081. doi:10.1080/15548627.2020.1810918, PMID:32804006.
- [7] Li Y, Yang W, Zheng Y, Dai W, Ji J, Wu L, *et al*. Targeting fatty acid synthase modulates sensitivity of hepatocellular carcinoma to sorafenib via ferroptosis. *J Exp Clin Cancer Res* 2023;42(1):6. doi:10.1186/s13046-022-02567-z, PMID:36604718.
- [8] Dixon SJ, Lemberg KM, Lamprecht MR, Skouta R, Zaitsev EM, Gleason CE, *et al*. Ferroptosis: an iron-dependent form of nonapoptotic cell death. *Cell* 2012;149(5):1060–1072. doi:10.1016/j.cell.2012.03.042, PMID:22632970.
- [9] Ji J, Wu L, Wei J, Wu J, Guo C. The Gut Microbiome and Ferroptosis in MAFLD. *J Clin Transl Hepatol* 2023;11(1):174–187. doi:10.14218/JCTH.2022.00136, PMID:36406312.
- [10] Pan Y, Wang X, Liu X, Shen L, Chen Q, Shu Q. Targeting Ferroptosis as a Promising Therapeutic Strategy for Ischemia-Reperfusion Injury. *Antioxidants (Basel)* 2022;11(11):2196. doi:10.3390/antiox11112196, PMID:36358568.
- [11] Wu S, Yang J, Sun G, Hu J, Zhang Q, Cai J, *et al*. Macrophage extracellular traps aggravate iron overload-related liver ischaemia/reperfusion in-

- jury. *Br J Pharmacol* 2021;178(18):3783–3796. doi:10.1111/bph.15518, PMID:33959955.
- [12] Buck-Wiese H, Andskog MA, Nguyen NP, Bligh M, Asmala E, Vidal-Melgosa S, *et al*. Fucoidan brown algae inject fucoidan carbon into the ocean. *Proc Natl Acad Sci U S A* 2023;120(1):e2210561119. doi:10.1073/pnas.2210561119, PMID:36584294.
- [13] Li J, Guo C, Wu J. Fucoidan: Biological Activity in Liver Diseases. *Am J Chin Med* 2020;48(7):1617–1632. doi:10.1142/S0192415X20500809, PMID:33148007.
- [14] Li J, Chen K, Li S, Liu T, Wang F, Xia Y, *et al*. Pretreatment with Fucoidan from *Fucus vesiculosus* Protected against ConA-Induced Acute Liver Injury by Inhibiting Both Intrinsic and Extrinsic Apoptosis. *PLoS One* 2016;11(4):e0152570. doi:10.1371/journal.pone.0152570, PMID:27035150.
- [15] de Melo K, Lisboa LDS, Queiroz MF, Paiva WS, Luchiari AC, Camara RBG, *et al*. Antioxidant Activity of Fucoidan Modified with Gallic Acid Using the Redox Method. *Mar Drugs* 2022;20(8):490. doi:10.3390/md20080490, PMID:36005493.
- [16] Apostolova E, Lukova P, Baldzhieva A, Delattre C, Molinier R, Petit E, *et al*. Structural Characterization and In Vivo Anti-Inflammatory Activity of Fucoidan from *Cystoseira crinita* (Desf.) Borry. *Mar Drugs* 2022;20(11):714. doi:10.3390/md20110714, PMID:36421993.
- [17] Wang L, Jayawardena TU, Hyun J, Wang K, Fu X, Xu J, *et al*. Antioxidant and anti-photoaging effects of a fucoidan isolated from *Turbinaria ornata*. *Int J Biol Macromol* 2023;225:1021–1027. doi:10.1016/j.ijbiomac.2022.11.164, PMID:36410533.
- [18] Irhimeh MR, Fitton JH, Lowenthal RM. Pilot clinical study to evaluate the anticoagulant activity of fucoidan. *Blood Coagul Fibrinolysis* 2009;20(7):607–610. doi:10.1097/MBC.0b013e32833135fe, PMID:19696660.
- [19] Chung HJ, Jeun J, Hwang SJ, Jun HJ, Kweon DK, Lee SJ. Toxicological evaluation of fucoidan from *Undaria pinnatifida* in vitro and in vivo. *Phytotherapy research* : PTR 2010;24(7):1078–1083. doi:10.1002/ptr.3138, PMID:20578121.
- [20] H K. *Biochemistry of sea algae*. *Cell physiol biochem* 1913;83(3):171–197.
- [21] Kim KJ, Lee OH, Lee BY. Genotoxicity studies on fucoidan from *Sporophyll of Undaria pinnatifida*. *Food Chem Toxicol* 2010;48(4):1101–1104. doi:10.1016/j.fct.2010.01.032, PMID:20138103.
- [22] Xue M, Tian Y, Sui Y, Zhao H, Gao H, Liang H, *et al*. Protective effect of fucoidan against iron overload and ferroptosis-induced liver injury in rats exposed to alcohol. *Biomed Pharmacother* 2022;153:113402. doi:10.1016/j.biopha.2022.113402, PMID:36076527.
- [23] Li J, Zhang Q, Li S, Dai W, Feng J, Wu L, *et al*. The natural product fucoidan ameliorates hepatic ischemia-reperfusion injury in mice. *Biomed Pharmacother* 2017;94:687–696. doi:10.1016/j.biopha.2017.07.109, PMID:28797984.
- [24] Sha Z, Yang Y, Liu R, Bao H, Song S, Dong J, *et al*. Hepatic Ischemia-reperfusion Injury in Mice was Alleviated by Rac1 Inhibition - More Than Just ROS-inhibition. *J Clin Transl Hepatol* 2022;10(1):42–52. doi:10.14218/JCTH.2021.00057, PMID:35233372.
- [25] Li J, Wang F, Xia Y, Dai W, Chen K, Li S, *et al*. Astaxanthin Pretreatment Attenuates Hepatic Ischemia Reperfusion-Induced Apoptosis and Autophagy via the ROS/MAPK Pathway in Mice. *Mar Drugs* 2015;13(6):3368–3387. doi:10.3390/md13063368, PMID:26023842.
- [26] Zhou J, Hu M, He M, Wang X, Sun D, Huang Y, *et al*. TNFAIP3 Interacting Protein 3 Is an Activator of Hippo-YAP Signaling Protecting Against Hepatic Ischemia/Reperfusion Injury. *Hepatology* 2021;74(4):2133–2153. doi:10.1002/hep.32015, PMID:34133792.
- [27] Shen W, Song Z, Zhong X, Huang M, Shen D, Gao P, *et al*. Sangerbox: A comprehensive, interaction-friendly clinical bioinformatics analysis platform. *iMeta* 2022;1(3):e36. doi:10.1002/imt2.36.
- [28] Oliveira C, Neves NM, Reis RL, Martins A, Silva TH. A review on fucoidan antitumor strategies: From a biological active agent to a structural component of fucoidan-based systems. *Carbohydr Polym* 2020;239:116131. doi:10.1016/j.carbpol.2020.116131, PMID:32414455.
- [29] Araya N, Takahashi K, Sato T, Nakamura T, Sawa C, Hasegawa D, *et al*. Fucoidan therapy decreases the proviral load in patients with human T-lymphotropic virus type-1-associated neurological disease. *Antivir Ther* 2011;16(1):89–98. doi:10.3851/IMP1699, PMID:21311112.
- [30] Monga SP. Lipid metabolic reprogramming in hepatic ischemia-reperfusion injury. *Nat Med* 2018;24(1):6–7. doi:10.1038/nm.4468, PMID:29315298.
- [31] R GB, Panisello-Rosello A, Sanchez-Nuno S, Alva N, Rosello-Catafau J, Carbonell T. Nrf2 and oxidative stress in liver ischemia/reperfusion injury. *FEBS J* 2022;289(18):5463–5479. doi:10.1111/febs.16336, PMID:34967991.
- [32] Wu S, Zhu J, Wu G, Hu Z, Ying P, Bao Z, *et al*. 6-Gingerol Alleviates Ferroptosis and Inflammation of Diabetic Cardiomyopathy via the Nrf2/HO-1 Pathway. *Oxid Med Cell Longev* 2022;2022:3027514. doi:10.1155/2022/3027514, PMID:36624878.
- [33] Tang W, Qin J, Zhou Y, Wang W, Teng F, Liu J, *et al*. Regulation of ferroptosis and ACSL4-15LO1 pathway contributed to the anti-asthma effect of acupuncture. *Int Immunopharmacol* 2023;115:109670. doi:10.1016/j.intimp.2022.109670, PMID:36603356.
- [34] Lin Z, Liu J, Long F, Kang R, Kroemer G, Tang D, *et al*. The lipid flipper SLC47A1 blocks metabolic vulnerability to ferroptosis. *Nat Commun* 2022;13(1):7965. doi:10.1038/s41467-022-35707-2, PMID:36575162.
- [35] Jiang J, Feng J, Song X, Yang Q, Zhao H, Zhao R, *et al*. Hsa_circ_0015278 Regulates FLT3-ITD AML Progression via Ferroptosis-Related Genes. *Cancers (Basel)* 2022;15(1):71. doi:10.3390/cancers15010071, PMID:36612069.
- [36] Chen J, Wang Y, Li M, Zhu X, Liu Z, Chen Q, *et al*. Netrin-1 Alleviates Early Brain Injury by Regulating Ferroptosis via the PPARgamma/Nrf2/GPX4 Signaling Pathway Following Subarachnoid Hemorrhage. *Transl Stroke Res* 2023. doi:10.1007/s12975-022-01122-4, PMID:36631632.
- [37] Xu WH, Li CH, Jiang TL. *Zhongguo Zhong Yao Za Zhi*. 2018;43(20):4019–4026. doi:10.19540/j.cnki.cjcm.20180517.001, PMID:30486525.
- [38] Qi D, Chen P, Bao H, Zhang L, Sun K, Song S, *et al*. Dimethyl fumarate protects against hepatic ischemia-reperfusion injury by alleviating ferroptosis via the NRF2/SLC7A11/HO-1 axis. *Cell Cycle* 2022;22(7):1–11. doi:10.1080/15384101.2022.2155016, PMID:36482709.
- [39] Tang D, Kroemer G. Ferroptosis. *Curr Biol* 2020;30(21):R1292–R1297. doi:10.1016/j.cub.2020.09.068, PMID:33142092.